ACS Macro Letters

Letter

Cite This: ACS Macro Lett. 2018, 7, 546−550

pubs.acs.org/macroletters

Consequences of Dispersity on the Self-Assembly of ABA-Type Amphiphilic Block Co-Oligomers

Anindita Das, Katja Petkau-Milroy,* Gilian Klerks, Bas van Genabeek, René P. M. Lafleur, Anja R. A. Palmans,* and E. W. Meijer*

Institute for Complex Molecular Systems and Laboratory of Macromolecular and Organic Chemistry, Eindhoven University of Technology, P.O. Box 513, 5600 MB Eindhoven, The Netherlands

Supporting Information

ABSTRACT: Intriguingly, little is known about the impact of dispersity on the crystallization driven self-assembly (CDSA) of amphiphilic block copolymers in aqueous media. Here, we investigate the influence of dispersity on the CDSA of ABA-type amphiphilic block co-oligomers (ABCOs). Two pairs of ABCOs are synthesized comprising discrete ($Đ$ = 1.00) or disperse ($Đ$ = 1.20) isotactic L-lactic acid 16-mers as the semicrystalline hydrophobic block and either oligo(ethylene glycol) methyl ether (MeOoEG) or oligo(tetraethylene glycol succinate) (oTEGSuc) as the discrete hydrophilic block. Self-assembly studies in water with 10% THF reveal uniform nanofibers/2D sheets for the discrete oligomers, but such structural regularity is largely compromised in the disperse oligomers. The results are corroborated by sharp melting transitions in both solution and bulk for the discrete ABCOs, unlike their disperse analogues that show a lack of crystallization. Interestingly, the discrete MeOoEG-LLA oligomer reveals crystallization driven gelation, illustrating the contrasting differences between the discrete oligomers and their disperse counterparts.

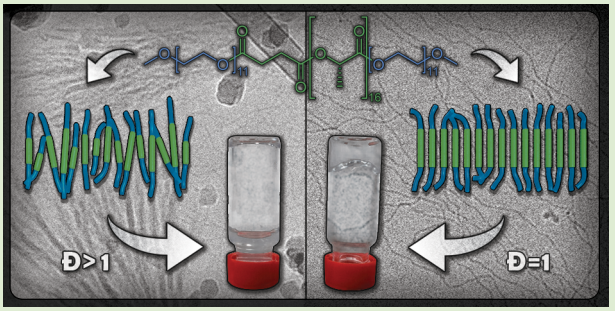

Self-assembly of block copolymers is a topic of considerable interest in polymer science due to the tremendous potential for applications in both biomedical engineering and nanolithography.[1,2] Although abiotic polymers synthesized via controlled polymerization techniques show great diversity in their structures and functions, they still suffer from significant molar mass distribution and cannot match up with the architectural purity, precision, and complexity displayed by biomacromolecules.[3,4] In contrast, most biopolymers such as DNA, RNA, and polypeptides are monodisperse and sequence-specific, which is critical to their overall three-dimensional organization and thus their properties and functions. In the recent past, polymer research started focusing on both discrete ($Đ$ < 1.000002)[4−10] and sequence-specific polymers[11−15] in an attempt to mimic these aspects of biomacromolecules.

Amphiphilic block copolymers (ABCPs) have been a topic of long-standing interest in biomedical research for their ability to form nanocarriers such as micelles, vesicles, nanorods, and other tailored shapes for drug delivery.[2,16,17] Depending on the hydrophilic/hydrophobic block ratio, molecular weight of the polymer, and crystallinity of the hydrophobic core, the morphology and properties of these nanoparticles can be engineered. Surprisingly, the impact of the molar mass distribution ($Đ$) on nanoparticle formation, shape, structural uniformity, and efficacy for uptake and release of guest molecules has hardly been investigated in amphiphilic block copolymers. Comparative self-assembly studies between ultra-defined discrete ABCPs ($Đ$ = 1.000) and their disperse counterparts could be extremely important in the fundamental understanding of the influence of dispersity on their properties after self-assembly in the aqueous phase. Contrasting differences between the discrete and disperse BCPs have been recently observed in the bulk phase. Our group has reported on the self-assembly of discrete diblock co-oligomers (BCOs) composed of oligolactic acid (oLA) and oligodimethylsiloxane (oDMS) obtained by iterative coupling-deprotection based synthetic strategies.[18,19] Whereas the discrete polymer formed well-organized lamellar structures, its disperse counterpart revealed a lower extent of ordering with an increase of the domain spacing and greater stability of the phase-separated structures.[19] In a complementary study, the group of Hawker observed similar differences in bulk between semidiscrete and disperse BCOs composed of oligomethyl methacrylate (oMMA) and oDMS.[20]

Intrigued by these results, we here aim to investigate the effect of dispersity in the aqueous phase, where the high mobility of the flexible polymers chains in solution presents an additional challenge. With this objective, we synthesized two pairs of ABA-type amphiphilic block co-oligomers (ABCOs) composed of discrete ($Đ$ = 1.000) or disperse ($Đ$ = 1.2)

Received: February 28, 2018
Accepted: April 4, 2018
Published: April 16, 2018

DOI: 10.1021/acsmacrolett.8b00168
ACS Macro Lett. 2018, 7, 546−550

isotactic oligo(L-lactic acid) (LLA) as the hydrophobic block and either oligoethylene glycol methyl ether (MeOoEG) or oligo(tetraethylene glycol succinate) (oTEGSuc) as the discrete hydrophilic block (Figure 1A). The rationale behind choosing

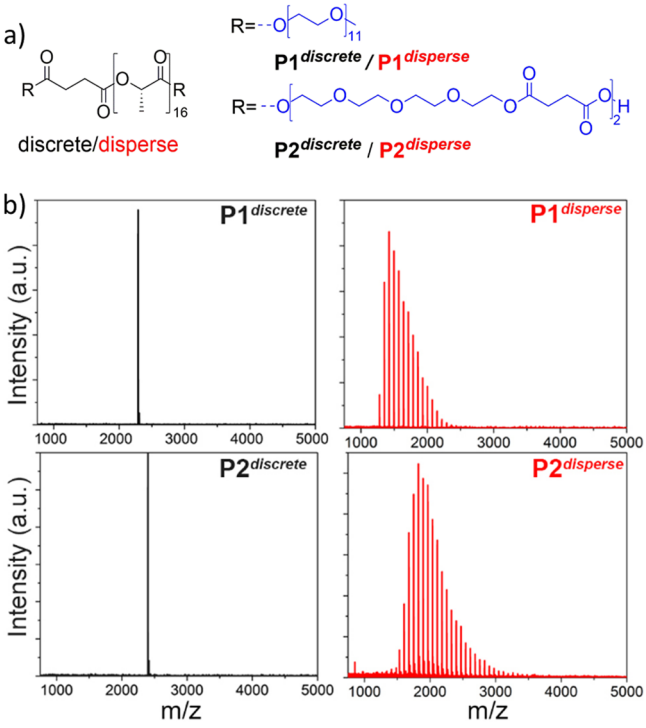

Figure 1. (a) Structures of discrete and disperse amphiphilic block co-oligomers and (b) their MALDI-ToF spectra.

these blocks is as follows: the self-assembly of polylactic acid-*b*-polyethylene glycol (PLA-*b*-PEG) has been explicitly studied[21−23] in the context of drug delivery and regenerative medicine because these polymers are known to be biocompatible.[24,25] oTEGSuc block was chosen as a biodegradable substitute to PEG, to generate fully biodegradable ABCOs.[26] Discrete chains of oTEGSuc can be synthesized following the iterative synthetic approach presented in Scheme 1. The L-lactic acid 16-mer was selected as the hydrophobic core either as a discrete 16-mer of exact molecular weight (LLA_{16}) or as a disperse one ($LLA_{\sim 16}$) with $Đ$ = 1.20. Discrete LLA_{16} is semicrystalline and forms ordered lamellae in the bulk.[27] In the context of drug delivery, the crystallization driven self-assembly (CDSA) of amphiphilic block copolymers with a crystallizable hydrophobic core has been applied to fabricate nonspherical nanostructures in solution.[28,29] However, as of yet there is no study on understanding the consequence of dispersity on block crystallinity in solution, which is investigated in the present work.

For the synthesis of discrete oTEGSuc, we followed a modified iterative coupling-deprotection route (Scheme 1a) recently reported by our group for monodisperse lactic acid oligomers.[18] Succinic acid monobenzyl ester (**1**) was coupled with mono *tert*-butyl dimethylsilyl (TBDMS) ether protected tetraethylene glycol (TEG; **2**) to obtain double-protected monomer $\mathbf{(TEGSuc)_1}$. Orthogonal deprotection of the TBDMS ether and the benzyl ester resulted in free hydroxyl and carboxylic acid containing **3** and **4**, respectively. Carbodiimide-promoted coupling between the two afforded double-protected dimer $\mathbf{(TEGSuc)_2}$. By repetition of the

Scheme 1. Synthesis of (a) Discrete Tetraethylene Glycol Succinate $(TEGSuc)_x$ Oligomers, (b) Their MALDI-ToF Spectra, and (c) Synthesis of Discrete ABCOs

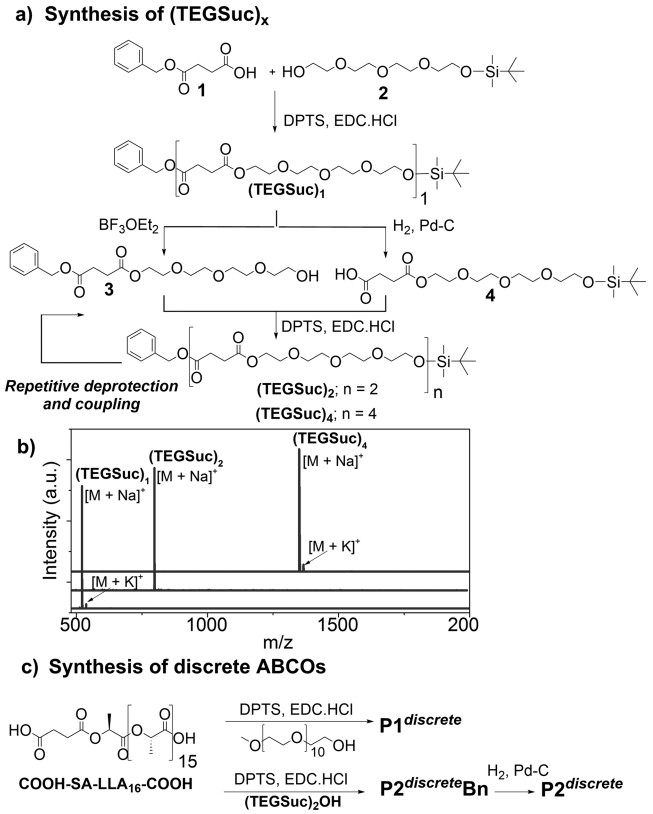

deprotection and coupling steps, tetramer $\mathbf{(TEGSuc)_4}$ was obtained. A stack plot of the MALDI-ToF spectra of the double-protected $\mathbf{(TEGSuc)_x}$ oligomers from monomer to tetramer is shown in Scheme 1b. Single peaks corresponding to the mass of the desired species complexed with sodium ion and potassium ion indicate that precisely defined block lengths were obtained.

The synthesis of discrete telechelic LLA_{16} with free carboxylic acid moieties (HOOC-SA-LLA_{16}-COOH, Scheme 1c) is based on the synthetic strategy previously reported by Hawker and co-workers.[30] Disperse telechelic $LLA_{\sim 16}$ was synthesized by ring-opening polymerization. The dispersity of $LLA_{\sim 16}$ ($Đ$ = 1.2) was determined using size exclusion chromatography. Full synthetic details on the preparation of the hydrophobic blocks can be found in the Supporting Information. Subsequent ligation of the acid functionalized LLA block with two equivalents of hydroxyl functionalized discrete $(TEGSuc)_2$-OH, or commercially available discrete $MeOoEG_{11}$−OH resulted in the target ABA-type ABCOs **P1** and **P2** (Scheme 1c). The discrete ABCOs are designated as $\mathbf{P}x^{discrete}$ and their disperse analogues are referred to as $\mathbf{P}x^{disperse}$. All the compounds were purified by automated column chromatography and fully analyzed by ^{1}H NMR, ^{13}C NMR, and matrix-assisted laser desorption/ionization time-of-flight (MALDI-ToF) mass spectrometry (Figures S1−S9). Despite similar degrees of polymerization based on ^{1}H NMR, the MALDI-ToF spectra of the discrete and the disperse oligomers reveal a wide distribution in the chain length for disperse samples compared to a single peak for the discrete ones (Figure 1).

The thermal behavior and degree of ordering in the bulk of the discrete and disperse ABCOs was investigated using

DOI: 10.1021/acsmacrolett.8b00168
ACS Macro Lett. 2018, 7, 546−550

differential scanning calorimetry (DSC; Figures S10 and S11) and small and wide angle X-ray scattering (SAXS and WAXS; Figure S12). The introduction of dispersity into the LLA block has a clear effect on the position and intensity of the DSC transitions for both the **P1** and **P2** systems (see SI for a detailed discussion). Notably, the SAXS data show a primary scattering peak only for the discrete samples, corresponding to d = 6.5 nm for **P1**^{discrete} and d = 10.5 nm for **P2**^{discrete}*Bn* (Figure S12). A higher order scattering peak at d = 5.2 nm in case of **P2**^{discrete}*Bn* suggests a lamellar packing of the ABCO in the bulk. Such clear scattering peaks at low q values are absent for both disperse **P1**^{disperse} and **P2**^{disperse}*Bn*, indicating reduced phase segregation between the two blocks and a less defined morphology. All in all, the differences in bulk properties of discrete and disperse ABCOs are in good correspondence to our previous results published on oLLA-oDMS block-*co*-oligomers,[19] where we observed a significant loss in long-range order when dispersity was introduced into the oLLA block.

Subsequently, the self-assembly of the ABCOs was studied in aqueous media. Due to the more hydrophobic nature of TEGSuc as compared to MeOoEG, **P2** could not be dissolved in pure water. As a result, all the studies were performed in water/THF mixtures with 10% THF.[31] To prepare the solutions, each compound was dissolved in THF, and water was added dropwise to reach a 1:9 THF/water binary mixture at 1−5 mg ABCO per mL. The formation of the nanoparticles was studied with light and X-ray scattering (LS and SAXS), micro-DSC, and microscopy (cryoTEM and total internal reflection fluorescence (TIRF) microscopy). Diffusion coefficients were obtained from multiangle light scattering by fitting the decay rate (Γ) versus the scattering vector (q) plot (Figure S13). Using the Stoke−Einstein equation, the hydrodynamic radius (R_h) of the particles was calculated. After self-assembly in water, the R_h was found to be larger for the discrete variants (R_h = 74 nm for **P1**^{discrete} and 125 nm for **P2**^{discrete}) than for the disperse analogues (R_h = 42 nm for **P1**^{disperse} and 90 nm for **P2**^{disperse}). When comparing the LS data of **P1** with **P2**, it appears that larger particles are for the **P2** pairs. However, fitting the decay rate versus the scattering vector reveals some anisotropy in the structures, indicating that the particles are not spherical, and thus, the Stoke−Einstein equation does not apply. To get an indication of the shape of the particles formed, the scattering intensity (I) was plotted against q (Figure S14). The slope of −1 for both **P1**^{discrete} and **P1**^{disperse} indicates that this ABCO self-assembles into cylindrical micelles, whereas **P2**^{discrete} and **P2**^{disperse} *self-assemble* into vesicles or flat bilayers (slope of −2). The morphology of an ABCP is largely dependent on the hydrophobic/hydrophilic block ratio.[2] For an invariant ratio, MeOoEG was replaced with a TEGSuc block of comparable molar mass. Possibly, the more hydrophobic nature of the TEGSuc block[26] changes this balance, leading to the formation of vesicles or bilayers.

To substantiate the formation of cylindrical micelles by **P1** in solution, SAXS measurements were performed. The SAXS profile obtained of **P1**^{discrete} was best fitted with a flexible cylinder model (Figures 2a and S15a). The radius of 3.2 nm, the Kuhn length of 103 nm and the overall length of 1038 nm agrees well with the cryoTEM observations (Figure 3b), which confirms the formation of elongated thin fibers of consistent width. In contrast, the cryoTEM image (Figure 3a) of the **P1**^{disperse} reveals the coexistence of two populations. Next to the elongated thin fibers, bundles of shorter but much wider fibers are present. This bundling effect might be due to the

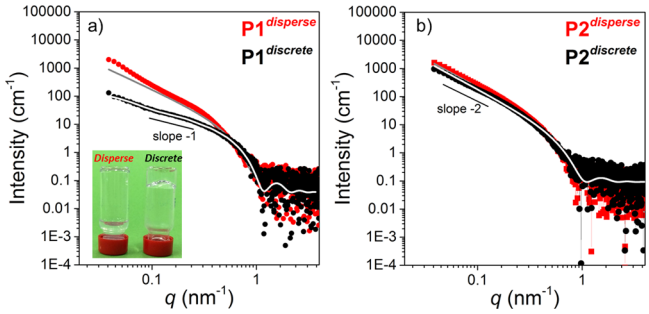

Figure 2. Solution SAXS traces of (a) **P1**^{discrete} and **P1**^{disperse} (0.5 mg mL^{-1}) and of (b) **P2**^{discrete} and **P2**^{disperse} (0.6 mg mL^{-1}) after self-assembly in water with 10% THF; (a, inset) self-assembly of **P1**^{discrete} (gel) and **P1**^{disperse} (sol) at 5 mg mL^{-1} in water with 10% THF. The lines represent the best fit to the data using either a flexible cylinder (a) or the lamellar (b) model.

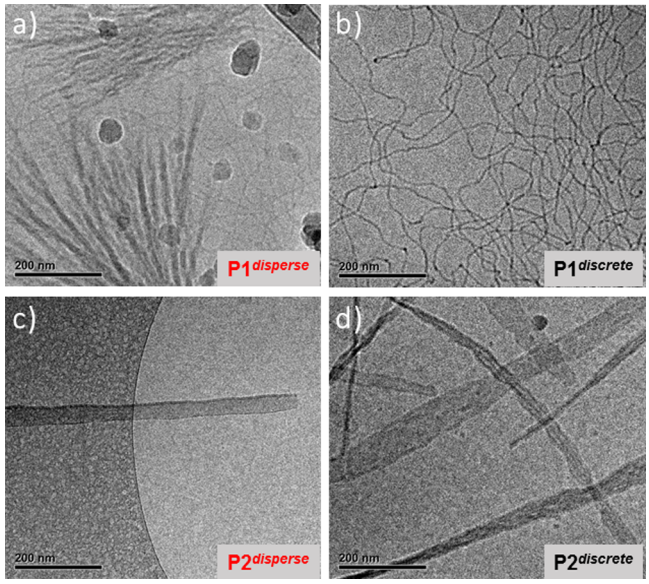

Figure 3. CryoTEM images at 25000 magnification of (a) **P1**^{disperse} and (b) **P1**^{discrete}, both at 5 mg mL^{-1} in water with 10% THF, and (c) **P2**^{disperse} and (d) **P2**^{discrete} both at 2 mg mL^{-1} in water with 10% THF. Large dark round particles in "a" are crystalline ice particles and not part of the sample. The images were recorded at 10 μm (a, b, d) and 5 μm defocus (c). For corresponding low-magnification images see Figure S17.

coassembly of LLA blocks of varying lengths. The SAXS profile of **P1**^{disperse} could not be fit well, which is likely due to an overlay of the scattering of multiple species present in solution (Figures 2a and S15b). The results above clearly exemplify the pronounced impact of LLA block dispersity on the homogeneity of the self-assembled structures. In addition, the morphologies formed were highly stable over time. CryoTEM images of aged samples for both **P1**^{discrete} and **P1**^{disperse} (Figure S16) retained the same morphologies even after keeping the solutions at room temperature for around 90 days.

Interestingly, the discrete oligomer **P1**^{discrete} formed a transparent gel at 5 mg mL^{-1} when the solution was heated and cooled back to room temperature (Figure 2a, inset). The gelation process was found to be reversible and repeatable. The gel−sol transition (T_{gel}), as determined visually for multiple cycles, varied between 42 and 48 °C upon heating the sample. This transition is very close to the melting temperature (T_m =

DOI: 10.1021/acsmacrolett.8b00168
ACS Macro Lett. 2018, 7, 546−550

41 °C) of discrete LLA_{16} block measured in the bulk (Figure S10a), as well as the transition temperature of 43 °C measured in solution by micro-DSC (Figure 4, vide infra). Notably, no

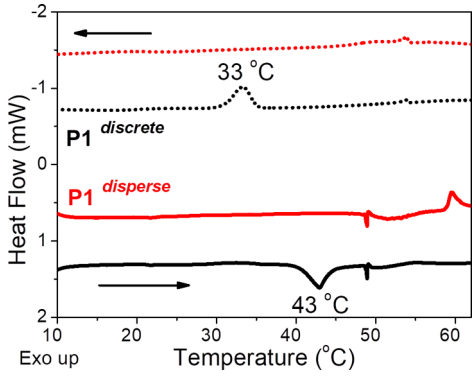

Figure 4. Micro-DSC traces of $\mathbf{P1}^{discrete}$ and $\mathbf{P1}^{disperse}$ at 5 mg mL^{-1} after self-assembly in water with 10% THF.

gelation was observed for $\mathbf{P1}^{disperse}$ under identical conditions, although gelation in disperse PEG-PLLA-PEG based triblock copolymer is well reported via interdigitation of micelles through PEG chains.[32] Such discrepancy in the gelation behavior of $\mathbf{P1}^{discrete}$ and $\mathbf{P1}^{disperse}$ nicely corroborates with their distinctly different morphologies as observed from cryoTEM.

The self-assembly of the **P2** pair was further investigated using SAXS in solution. The SAXS profile for both $\mathbf{P2}^{discrete}$ and $\mathbf{P2}^{disperse}$ shows a slope of −2, indicating the formation of vesicles or flat bilayers (Figures 2b and S15c,d). In contrast to the **P1** pair, both profiles for $\mathbf{P1}^{discrete}$ and $\mathbf{P1}^{disperse}$ are very similar. The SAXS profiles were fitted best using the lamellae model, indicating a lamellae thickness of 7 nm ($\mathbf{P2}^{discrete}$) or 8 nm ($\mathbf{P2}^{disperse}$). Since the $\mathbf{P2}^{disperse}$ sample was not transparent, indicative of the formation of large aggregates, cryoTEM imaging of $\mathbf{P2}^{disperse}$ was first performed of a filtered sample, revealing the presence of uniform sheets rolled into U-shape (Figures 3c and S18). Flat sheets were observed in a sample that was not filtered prior to imaging (Figure S18). To visualize the aggregates of $\mathbf{P2}^{disperse}$ at the μm length scale, TIRF microscopy was performed after the addition of the dye Nile Red. This hydrophobic dye is weakly fluorescent in water but becomes highly fluorescent after incorporation into hydrophobic domains.[33] Besides the sheets rolled into U-shape, other spherical morphologies and large aggregates were present (Figure S18). In contrast, for $\mathbf{P2}^{discrete}$ only the formation of long sheets was observed by cryoTEM imaging (Figure 3d), as well as by TIRF microscopy (Figure S19). Also for the **P2** set, the results clearly exemplify that the dispersity of the $LLA_{\sim 16}$ block inhibits the uniformity of the self-assembled structures in solution.

To study whether the self-assembly in solution is driven by the crystallization of the LLA block, microdifferential scanning calorimetry (microDSC) in 1:9 THF/water was performed. The solutions were heated from 5 to 70 °C at a rate of 0.5 K min^{-1} (Figure 4). $\mathbf{P1}^{discrete}$ showed clear endothermic and exothermic transitions in the heating and the cooling runs corresponding to melting (T_m = 43 °C) and crystallization (T_c = 33 °C), respectively. The T_m in solution (Figure 4) corresponds well with the melting (T_m = 41 °C) in bulk (Figure S10a) for $\mathbf{P1}^{discrete}$ indicating that this transition is indeed connected to the LLA_{16} crystallization. Further, close matching of the T_m with the $T_{gel-sol}$ of $\mathbf{P1}^{discrete}$ substantiates crystallization driven gelation. Interestingly, no phase transitions were observed for the discrete $\mathbf{P2}^{discrete}$ (Figure S20), suggesting that the change in the hydrophilic block from MeOoEG to TEGSuc might influence the crystallization of the LLA_{16} core. This corroborates well with the amorphous nature of TEGSuc block as observed from its DSC profile (Figure S11a) in contrast to the semicrystalline PEG chain (Figure S11b). The very slow rate of crystallization of $\mathbf{P2}^{discrete}$*Bn* in the bulk (Figure S10b,c) further supports our interpretation that the PEG chains aid the ordering of the LLA_{16} block unlike TEGSuc chains for discrete pairs.

No clear transitions were observed for $\mathbf{P1}^{disperse}$ (Figure 4) or $\mathbf{P2}^{disperse}$ (Figure S20). Such distinct differences between $\mathbf{P1}^{discrete}$ and $\mathbf{P1}^{disperse}$ reveal the negative impact of dispersity on the core crystallinity of the amphiphiles in the solution phase, leading to their varying self-assembly behavior. Possibly, the dispersity in the hydrophobic block does not allow effective packing of the LLA chains of varying length within the core of the nanoparticles in $\mathbf{P1}^{disperse}$, unlike in $\mathbf{P1}^{discrete}$. Although there are multiple reports on crystallization driven self-assembly of block copolymer amphiphiles, this is the first demonstration of the consequence of dispersity on the crystallization mediated self-assembly of oligomeric amphiphiles in aqueous solution.

In summary, we have methodically manifested the effect of dispersity on the assembly behavior of two sets of discrete amphiphilic block co-oligomers by comparing their solution self-assembly behaviors with their disperse counterparts. The finding of this work reveals remarkable differences between the discrete and the disperse ABCOs not just in the bulk but also in the solution phase in terms of crystallinity, gelation, morphology, and homogeneity of the self-assembled structures. We anticipate that further fundamental studies on pharmaceutically relevant PEG−PLLA based block co-oligomers will pave the way for synthesis of tailor-made nanocarriers with more control over their structures, dynamics, and functions as delivery vehicles.

■ ASSOCIATED CONTENT

Supporting Information

The Supporting Information is available free of charge on the ACS Publications website at DOI: 10.1021/acsmacrolett.8b00168.

Experimental procedures, synthesis, and characterization data for all compounds, bulk characterization, and Figures S1−S20 (PDF).

■ AUTHOR INFORMATION

Corresponding Authors

*E-mail: e.w.meijer@tue.nl.
*E-mail: a.palmans@tue.nl.
*E-mail: k.petkau-milroy@tue.nl.

ORCID

Anja R. A. Palmans: 0000-0002-7201-1548
E. W. Meijer: 0000-0003-4126-7492

Author Contributions

All authors have given approval to the final version of the manuscript.

Notes

The authors declare no competing financial interest.

DOI: 10.1021/acsmacrolett.8b00168
ACS Macro Lett. 2018, 7, 546−550

■ ACKNOWLEDGMENTS

The authors acknowledge financial support from the Dutch Ministry of Education, Culture and Science (Gravity Program 024.001.035). The BM29 beamline at the European Synchrotron Radiation Facilities (Grenoble, France) is acknowledged for access to the synchrotron facilities and for help with acquiring SAXS data. We gratefully thank G.M. ter Huurne for his help of acquiring the SAXS data and S. P. W. Wijnands for his help with TIRF microscopy.

■ REFERENCES

(1) Whitesides, G. M.; Boncheva, M. Beyond Molecules: Self-Assembly of Mesoscopic and Macroscopic Components. *Proc. Natl. Acad. Sci. U. S. A.* **2002**, *99*, 4769−4774.
(2) Mai, Y.; Eisenberg, A. Self-Assembly of Block Copolymers. *Chem. Soc. Rev.* **2012**, *41*, 5969.
(3) Lutz, J.-F.; Lehn, J.-M.; Meijer, E. W.; Matyjaszewski, K. From Precision Polymers to Complex Materials and Systems. *Nat. Rev. Mater.* **2016**, *1*, 16024.
(4) Hawker, C. J.; Wooley, K. L. The Convergence of Synthetic Organic and Polymer Chemistries. *Science* **2005**, *309*, 1200−1205.
(5) Lawrence, J.; Lee, S.-H.; Abdilla, A.; Nothling, M. D.; Ren, J. M.; Knight, A. S.; Fleischmann, C.; Li, Y.; Abrams, A. S.; Schmidt, B. V. K. J.; Hawker, M. C.; Connal, L. A.; McGrath, A. J.; Clark, P. G.; Gutekunst, W. R.; Hawker, C. J. A Versatile and Scalable Strategy to Discrete Oligomers. *J. Am. Chem. Soc.* **2016**, *138*, 6306−6310.
(6) Takizawa, K.; Tang, C.; Hawker, C. J. Molecularly Defined Caprolactone Oligomers and Polymers: Synthesis and Characterization. *J. Am. Chem. Soc.* **2008**, *130*, 1718−1726.
(7) Jiang, Y.; Golder, M. R.; Nguyen, H. V.-T.; Wang, Y.; Zhong, M.; Barnes, J. C.; Ehrlich, D. J. C.; Johnson, J. A. Iterative Exponential Growth Synthesis and Assembly of Uniform Diblock Copolymers. *J. Am. Chem. Soc.* **2016**, *138*, 9369−9372.
(8) Yang, J.; Gitlin, I.; Krishnamurthy, V. M.; Vazquez, J. A.; Costello, C. E.; Whitesides, G. M. Synthesis of Monodisperse Polymers from Proteins. *J. Am. Chem. Soc.* **2003**, *125*, 12392−12393.
(9) Székely, G.; Schaepertoens, M.; Gaffney, P. R. J.; Livingston, A. G. Beyond PEG2000: Synthesis and Functionalisation of Monodisperse PEGylated Homostars and Clickable Bivalent Polyethyleneglycols. *Chem. - Eur. J.* **2014**, *20*, 10038−10051.
(10) Williams, J. B.; Chapman, T. M.; Hercules, D. M. Synthesis of Discrete Mass Poly(butylene glutarate) Oligomers. *Macromolecules* **2003**, *36*, 3898−3908.
(11) Rosales, A. M.; Segalman, R. A.; Zuckermann, R. N. Polypeptoids: A Model System to Study the Effect of Monomer Sequence on Polymer Properties and Self-Assembly. *Soft Matter* **2013**, *9*, 8400−8414.
(12) Lutz, J.-F. J.-F. Sequence-Controlled Polymerizations: The next Holy Grail in Polymer Science? *Polym. Chem.* **2010**, *1*, 55−62.
(13) Ida, S.; Ouchi, M.; Sawamoto, M. Template-Assisted Selective Radical Addition toward Sequence-Regulated Polymerization: Lariat Capture of Target Monomer by Template Initiator. *J. Am. Chem. Soc.* **2010**, *132*, 14748−14750.
(14) Lutz, J.-F. Defining the Field of Sequence-Controlled Polymers. *Macromol. Rapid Commun.* **2017**, *38*, 1700582.
(15) Robertson, E. J.; Battigelli, A.; Proulx, C.; Mannige, R. V.; Haxton, T. K.; Yun, L.; Whitelam, S.; Zuckermann, R. N. Design, Synthesis, Assembly, and Engineering of Peptoid Nanosheets. *Acc. Chem. Res.* **2016**, *49*, 379−389.
(16) Pijpers, I. A. B.; Abdelmohsen, L. K. E. A.; Williams, D. S.; van Hest, J. C. M. Morphology Under Control: Engineering Biodegradable Stomatocytes. *ACS Macro Lett.* **2017**, *6*, 1217−1222.
(17) Abdelmohsen, L. K. E. A.; Williams, D. S.; Pille, J.; Ozel, S. G.; Rikken, R. S. M.; Wilson, D. A.; van Hest, J. C. M. Formation of Well-Defined, Functional Nanotubes via Osmotically Induced Shape Transformation of Biodegradable Polymersomes. *J. Am. Chem. Soc.* **2016**, *138*, 9353−9356.
(18) van Genabeek, B.; de Waal, B. F. M.; Gosens, M. M. J.; Pitet, L. M.; Palmans, A. R. A.; Meijer, E. W. Synthesis and Self-Assembly of Discrete Dimethylsiloxane−Lactic Acid Diblock Co-Oligomers: The Dononacontamer and Its Shorter Homologues. *J. Am. Chem. Soc.* **2016**, *138*, 4210−4218.
(19) van Genabeek, B.; de Waal, B. F. M.; Ligt, B.; Palmans, A. R. A.; Meijer, E. W. Dispersity under Scrutiny: Phase Behavior Differences between Disperse and Discrete Low Molecular Weight Block Co-Oligomers. *ACS Macro Lett.* **2017**, *6*, 674−678.
(20) Oschmann, B.; Lawrence, J.; Schulze, M. W.; Ren, J. M.; Anastasaki, A.; Luo, Y.; Nothling, M. D.; Pester, C. W.; Delaney, K. T.; Connal, L. A.; et al. Effects of Tailored Dispersity on the Self-Assembly of Dimethylsiloxane−Methyl Methacrylate Block Co-Oligomers. *ACS Macro Lett.* **2017**, *6*, 668−673.
(21) Yang, J.; Liang, Y.; Luo, J.; Zhao, C.; Han, C. C. Multilength Scale Studies of the Confined Crystallization in Poly(L-lactide)-*b*-Poly(ethylene glycol) Copolymer. *Macromolecules* **2012**, *45* (10), 4254−4261.
(22) Zhang, J.; Wang, L.-Q.; Wang, H.; Tu, K. Micellization Phenomena of Amphiphilic Block Copolymers Based on Methoxy Poly(ethylene glycol) and Either Crystalline or Amorphous Poly(caprolactone-*b*-lactide). *Biomacromolecules* **2006**, *7*, 2492−2500.
(23) Heald, C. R.; Stolnik, S.; Kujawinski, K. S.; De Matteis, C.; Garnett, M. C.; Illum, L.; Davis, S. S.; Purkiss, S. C.; Barlow, R. J.; Gellert, P. R. Poly(lactic acid)−Poly(ethylene oxide) (PLA−PEG) Nanoparticles: NMR Studies of the Central Solidlike PLA Core and the Liquid PEG Corona. *Langmuir* **2002**, *18*, 3669−3675.
(24) Knop, K.; Hoogenboom, R.; Fischer, D.; Schubert, U. S. Poly(ethylene glycol) in Drug Delivery: Pros and Cons as Well as Potential Alternatives. *Angew. Chem., Int. Ed.* **2010**, *49*, 6288−6308.
(25) Nicolas, J.; Mura, S.; Brambilla, D.; Mackiewicz, N.; Couvreur, P. Design, Functionalization Strategies and Biomedical Applications of Targeted Biodegradable/biocompatible Polymer-Based Nanocarriers for Drug Delivery. *Chem. Soc. Rev.* **2013**, *42*, 1147−1235.
(26) Chen, S.; Wang, Y.; Fan, Y.; Ma, J. Synthesis of Amphiphilic Poly(tetraethylene glycol succinate) and the Thermosensitivity of Its Aggregation in Water. *J. Biomed. Mater. Res., Part A* **2009**, *88A*, 769−777.
(27) van Genabeek, B.; Lamers, B. A. G.; de Waal, B. F. M.; van Son, M. H. C.; Palmans, A. R. A.; Meijer, E. W. Amplifying (Im)perfection: The Impact of Crystallinity in Discrete and Disperse Block Co-Oligomers. *J. Am. Chem. Soc.* **2017**, *139*, 14869−14872.
(28) Gilroy, J. B.; Gädt, T.; Whittell, G. R.; Chabanne, L.; Mitchels, J. M.; Richardson, R. M.; Winnik, M. A.; Manners, I. Monodisperse Cylindrical Micelles by Crystallization-Driven Living Self-Assembly. *Nat. Chem.* **2010**, *2*, 566−570.
(29) Pitto-Barry, A.; Kirby, N.; Dove, A. P.; O'Reilly, R. K. Expanding the Scope of the Crystallization-Driven Self-Assembly of Polylactide-Containing Polymers. *Polym. Chem.* **2014**, *5*, 1427−1436.
(30) Takizawa, K.; Nulwala, H.; Hu, J.; Yoshinaga, K.; Hawker, C. J. Molecularly Defined (L)-Lactic Acid Oligomers and Polymers: Synthesis and Characterization. *J. Polym. Sci., Part A: Polym. Chem.* **2008**, *46*, 5977−5990.
(31) $\mathbf{P1}^{discrete}/\mathbf{P1}^{disperse}$ show higher solubility (up to 5 mg mL^{-1} instead of only 2 mg mL^{-1} for $\mathbf{P2}^{discrete}/\mathbf{P2}^{disperse}$) and are soluble in pure water as well.
(32) Jeong, B.; Bae, Y. H.; Lee, D. S.; Kim, S. W. Biodegradable Block Copolymers as Injectable Drug-Delivery Systems. *Nature* **1997**, *388*, 860.
(33) Sackett, D. L.; Wolff, J. Nile Red as a Polarity-Sensitive Fluorescent Probe of Hydrophobic Protein Surfaces. *Anal. Biochem.* **1987**, *167*, 228−234.

DOI: 10.1021/acsmacrolett.8b00168
ACS Macro Lett. 2018, 7, 546−550